# Applications of environmental scanning electron microscopy to colloidal aggregation and film formation

Athene M. Donald *, Chaobin He, C. Patrick Royall, Michele Sferrazza, Nadia A. Stelmashenko, Bradley L. Thiel

*Cavendish Laboratory, Department of Physics, University of Cambridge, Madingley Road, Cambridge CB3 OHE, UK*

**Abstract**

Environmental scanning electron microscopy (ESEM) is a rather new form of electron microscopy, which permits the observation of hydrated samples in their native state, and also does not require that insulators are coated with a conducting layer. These two factors make it ideal for studying colloidal dispersions as they aggregate and/or film form. This paper describes the application of ESEM to three situations involving aggregating latices. Firstly the nature of fractal structures grown from aggregating acrylic latices is discussed, with a comparison given of the behaviour with and without added salt as the screening between particles is altered. Secondly the behaviour of vinyl latices is considered. The impact of the addition of starch, both modified and unmodified, upon the particle size distribution and ability to film form is examined. Finally, the structures which form when the hard inorganic component silica is added to acrylic latices are explored. Together these three examples illustrate some of the many strengths of the ESEM in the field of colloidal dispersions and aggregates. © 2000 Elsevier Science B.V. All rights reserved.

*Keywords:* Environmental scanning electron microscopy; Colloidal aggregation; Film formation

## 1. Introduction

For many colloidal systems, water is an integral part of the whole, and as such the ability to image 'wet' systems in their native state is vital. However there is a dearth of techniques which combine this wet-imaging ability with good resolution and depth of field. Optical microscopy has a long and distinguished history, but for smaller colloidal particles its resolution is frequently inadequate. Conversely electron microscopy has, until re-cently, been limited by the need to carry out examination of a sample in the high vacuum required by the instruments (be they scanning or transmission electron microscopes, SEMs or TEMs, respectively). Due to this limitation it has always been necessary to go through a series of fairly drastic specimen preparation steps such as freeze-drying prior to imaging. This leads to the danger that artefacts may creep into the image perhaps because of ice crystal formation, or that redistribution of components could occur during the freeze-drying process. For these reasons there has been a need for a microscopy which permits

* Corresponding author. Fax: + 44-1223-337000.

the imaging of colloidal dispersions in their native state, yet still with the high resolution of an electron microscope. The introduction of the environmental scanning electron microscope (ESEM) in the last decade, and its various cousins at the low vacuum end (known variously as leaky SEMs, low vacuum SEMs, variable pressure SEMs etc) has now opened up the field. However, comparatively little work has yet been done utilising the full power of the instrument for colloidal systems, not least because of a failure of an appreciation of the potential of the instrument. This article serves to highlight the power of the technique, in the hopes that other workers in the field will feel encouraged to apply it to their particular favourite colloid, and to demonstrate its applicability to a few specific examples in the field of particle aggregation and coalescence. A brief overview of the limited applications of ESEM to colloids in the literature can be found in Donald [1].

So how is it possible to keep water in an electron microscope and still form a high resolution image? The key development lay in the recog-

nition by Danilatos that by utilising a column with a system of differential pumping zones, it was possible to satisfy both the requirement that the electron gun was kept at the necessary high vacuum, and that the sample was kept wet (for a useful early review see Danilatos [2]). Fig. 1 shows a schematic of the lay-out of the column, with the different pressure zones identified. The vacuum considerations in the vicinity of the gun are sufficient to permit a $LaB_6$ filament to be used, with its high brightness, as well as the more common tungsten filament. Below the gun are a series of pressure-limiting apertures (typically three) across which there is differential pumping to allow a pressure difference to be maintained. In this way a pressure of up to about 20 torr ($\sim 1000$ Pa) can be maintained in the vicinity of the sample. As we will see below, this is sufficient to ensure that a wet sample can be maintained in its wet state.

However maintaining this pressure differential is not in itself sufficient to permit the operation of the instrument. There are two further requirements: firstly to ensure that the scattering which the electron beam undergoes as it passes through
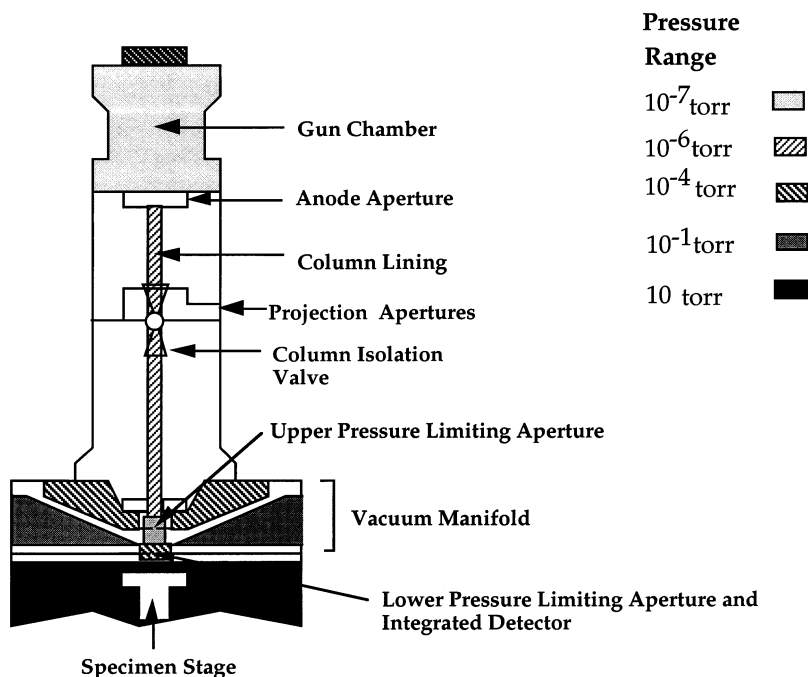


Fig. 1. Schematic of the ESEM column, identifying the different pressure regimes.

a)        **incident probe beam**

b)

**sharp central probe** ←

**broad skirt surrounds the central probe**
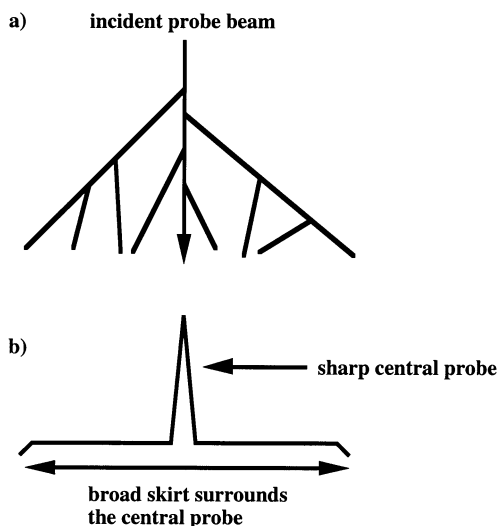
Fig. 2. Scattering of the incident beam by the gas molecules causes a so-called 'skirt' to form, but the central probe is still sharp: (a) the incident beam undergoes collisions but most of the electrons travel unscattered; (b) the shape of the probe which forms as a result.

positively charged detector

incident electron beam

cascade electrons

positive ion

gaseous atom

earthed sample
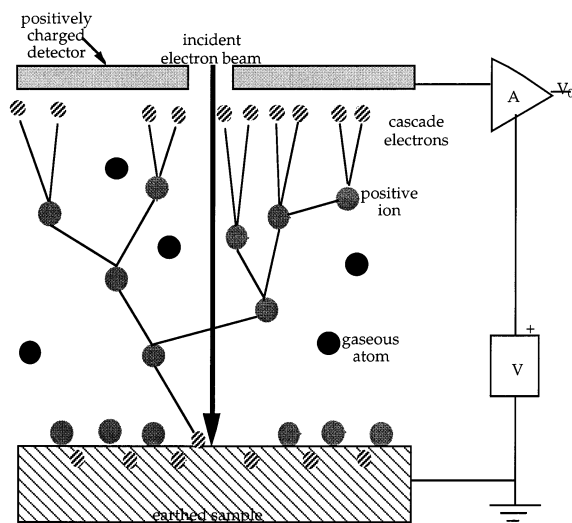
Fig. 3. Schematic representation of the cascade amplification process, whereby daughter electrons are created en route to the detector.

a region containing gas molecules is not so great to degrade the image resolution to the point that it is no longer better than an optical microscope (for instance); and secondly to build a detector

that is capable of operating outside a vacuum. The requirement that the scattering is not excessive is most easily met by ensuring that the distance from the final pressure-limiting aperture to the sample is only short, the so-called working distance. As long as the average number of collisions an electron in the primary beam undergoes as it travels that distance is kept small, and indeed that the majority of the electrons are not scattered at all, the net effect is to introduce a broad 'skirt' onto a sharp and well-defined probe as can be seen in Fig. 2. This skirt effectively acts as a DC background, but does not significantly degrade the resolution. To ensure that this so-called oligoscattering regime is not exceeded, the combination (crudely this can be represented by the product) of working distance and chamber pressure needs to be kept sufficiently low. This naturally imposes restrictions on the possible conditions within the chamber, and hence the experiments that can be carried out. However, as we will see below, it nevertheless leaves a broad and extremely useful window within which wet samples can readily be imaged.

As regards the detector, Danilatos back in the early 1980s designed a simple and effective detector, quite distinct from the Everhardt–Thornley detector used in conventional SEMs, known as the environmental secondary electron detector. Since then detectors have continued to evolve, and are still doing so as our understanding of how to optimise signal detection continues to improve. For all the detectors the basic principles are the same. Electrons emitted from the sample, be they secondary electrons or the higher energy backscattered, have to travel back through the gas-containing chamber to the detector. In traversing the gas, these electrons will undergo collisions with the gas molecules. The collisions may be of various types both inelastic and elastic. Of crucial importance are the ionising collisions which lead to the creation of new daughter electrons. In this way a cascade amplification process occurs as shown in Fig. 3, so that many more electrons are detected than were originally emitted from the sample. The degree of amplification has been studied in detail, Fletcher et al. [3], Thiel et al. [4], and depends on operating parameters such as gas

pressure and working distance. A highly desirable side effect of the cascade amplification process is that positive ions are formed which drift back to the surface of the sample. There they can neutralise the usual build-up of charge associated with electron microscopy of insulators. This means that insulating samples can be viewed without the need to apply any conducting coating first. A corollary of this is that fine surface detail can be seen without the risk of it being obscured by a thin conductive layer.

All these instrumental developments will not avail the study of wet dispersions unless control can be obtained over the state of the sample. There are two necessary problems to overcome here: maintaining the sample in its wet state as the whole instrument is pumped down from ambient to a few torr in the chamber, and thereafter ensuring that dehydration does not occur during the period of imaging. The former condition can be met by suitable control of the way evacuation is carried out, performing this in steps to maintain as high a percentage of water in the chamber as possible at each step, (Cameron and Donald [5]). To ensure that the second condition is met it is necessary to consider the form of the saturated vapour pressure curve (SVP) for water as a function of temperature, as shown in Fig. 4. From this curve it can be seen that at room temperature it is not possible to maintain SVP simultaneously whilst having a low enough vapour pressure (say less than 10 torr) in the chamber to provide a decent resolution image. The solution to this
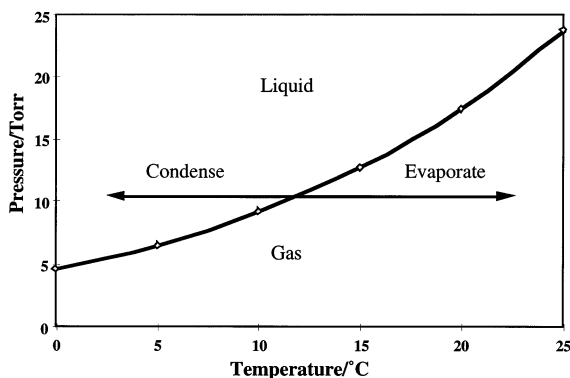
problem is to cool the sample slightly to a few degrees centigrade. At a temperature of $\sim 6°C$ a pressure of 6 torr will be sufficient to maintain SVP and hence prevent loss of water from the sample. Therefore by using a Peltier cooling stage to control the temperature slightly below ambient, and by appropriate control of the chamber pressure, not only can the sample be maintained wet but it is also possible systematically to permit either hydration or dehydration experiments to be carried out whilst continuing to image the sample. Examples of the utility of these procedures will be given below.

This article aims to illustrate by suitable examples from the work at the Cavendish the great potential power of the technique of ESEM for colloids. Three illustrative examples are presented here in some depth in order to achieve this goal. The experiments were carried out on either an Electroscan E3 model, operating with a $LaB_6$ filament, or a 2010 model with a tungsten filament. In both cases a Peltier cooling stage was used, as indicated above, to ensure correct control of the combination of sample temperature and chamber pressure so that the position of the sample relative to the SVP curve was known. Although in principle gases other than water can be used in the chamber (Fletcher et al. [3]), for samples where the state of hydration is crucial water is obviously the gas of choice and has been used in all the experiments described here.

## 2. Aggregation of non-film forming PMMA latices

### 2.1. Experimental

The majority of the experiments described here were performed on a latex comprising core-shell rubber particles supplied by ICI plc: each particle had a poly methyl methacrylate (PMMA) core, a rubber middle layer and a PMMA outer layer, with an overall dimension of 0.25 μm. Particles were dispersed in water containing $MgSO_4$ at a concentration ranging from 0 to 0.25 M. The temperature of the stage was maintained at around 2°C; initially conditions were set so that

Fig. 4. Saturated vapour pressure curve (SVP) curve for water.
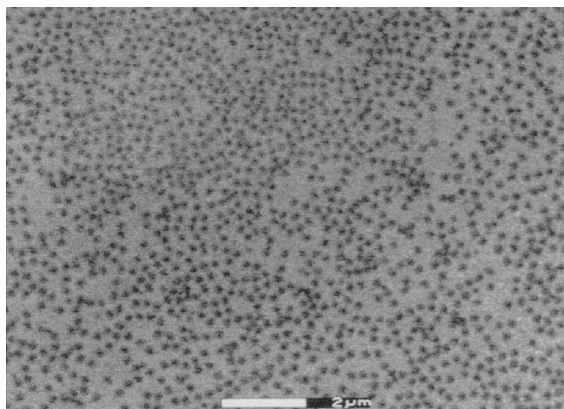
Fig. 5. Acrylic latex in water.
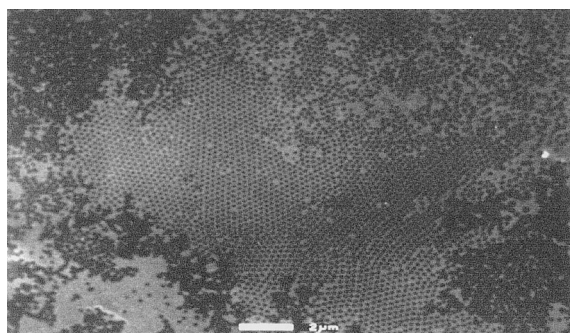


Fig. 6. As water is allowed to evaporate in the ESEM, a colloidal crystal starts to form from the acrylic latex.

no evaporation or condensation occurred. After this initial imaging the temperature was raised slightly so that evaporation took place whilst imaging was continued. In this way the evolving structure during aggregation could be followed in real time. A few experiments were also carried out on a similar particle, but lacking the outside layer of PMMA. It is, therefore, a 'soft' latex in so far as the outer layer has a $T_g$ of below zero. In principle videos can be taken in real time of the whole process, so that each stage can be examined in detail later. In practice the danger of beam damage affecting the response of the system, if a given area is viewed for extended periods, means videoing must be treated with caution.

## 2.2. Results and discussion

Fig. 5 shows an example of the latex dispersion before any drying has occurred. The individual particles are well resolved, and their apparent 'fuzziness' in places is due to the fact that they are dispersed in water (and hydrated particles will always have a more diffuse boundary than dry) and are undergoing Brownian motion on the time scale of the recording time for the frame (some seconds). It must be remembered that what this image shows is the surface only of the sample. Thus what can be seen is where individual particles are protruding through the surface or covered by only a sufficiently thin layer of water that the electron beam can penetrate. Thus all the grey regions in between the individual particles correspond to water where there are no particles close enough to the surface to be visible. At this early stage the particles remain distinct, and there are no aggregates visible.

As evaporation proceeds, aggregation begins (Fig. 6). In this case, where no salt is present, watching the particle collisions shows that a collision does not usually lead to 'sticking,' i.e. a particle joining an aggregate. The net result is the slow formation of a well-ordered colloidal crystal. In the surface plane the majority of the packing is found to have hexagonal symmetry, although occasionally four-fold symmetry is also seen (He and Donald [6]). The packing is seen to have many defects, both in terms of 'missing' particles, and in terms of grain boundaries where the orientation of the planes changes.

In the presence of salt, the structures which form are much less ordered. Systematic changes can be seen as the molarity of the $MgSO_4$ is raised, (He and Donald [6]). The addition of salt has the effect of reducing the long-range repulsion so that the barrier to the deep primary minimum of the interparticle potential is reduced. When two particles come together the probability of sticking therefore increases and this can be directly viewed in the ESEM with the particles coming together in the primary minimum. This aggregation will be irreversible (Jeffrey and Ottewill [7]). The net effect is therefore to lead to a much more disordered, open structure than in the no-salt case.

Fig. 7 compares the form of the flocs that form for the case of 0.078 and 0.25 M $MgSO_4$, for the same overall particle concentration of $1 \times 10^{13}$ particles $cm^{-3}$. It can be seen that a much more compact structure is formed for the latter case than for the former, and in neither case is there any regularity of packing of the type seen in the colloidal crystals when no salt is present. Images such as those seen in Fig. 7 can be analysed in more detail to provide a novel way of characterising the fractal dimension of the flocs that form.

a)



b)
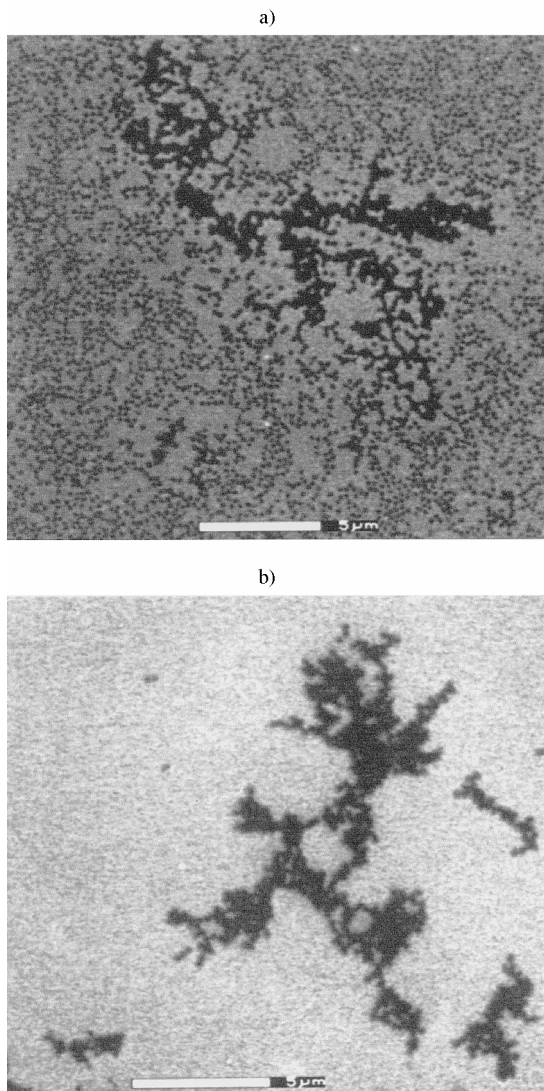


Fig. 7. Flocs formed during the evaporation of water from a latex containing (a) 0.078 M $MgSO_4$ and (b) 0.25 M $MgSO_4$.

The fractal (or Hausdorff) dimension $d$ is a measure of how convoluted the fractal structure is. Its value depends on the mechanism by which the fractal structure has formed. Colloidal aggregation is usually described by one of three limiting case models: fast diffusion limited cluster aggregation (DLCA), slow reaction limited cluster aggregation (RLCA) and diffusion limited aggregation (DLA) (Weitz [8]). In the RLCA case there are significant repulsive forces acting between neighbours, with the consequence of producing slow aggregation rates and more compact structures than in the DLCA case. Diffusion limited aggregation (DLA) idealises the irreversible aggregation of colloidal particle aggregates, in which individual particles join pre-existing clusters. This is in contrast to the DLCA regime, in which clusters diffuse to join other, pre-existing clusters. According to theory and simulation, the fractal dimension of two dimensional flocs should be 1.45 for the DLCA regime, 1.6 for the RLCA regime and 1.7 for DLA aggregation (Witten and Sander [9], Viscek [10]), although experimental results are not so clear cut (Richetti et al. [11], Hurd and Schaefer [12], Stannkiewicz et al. [13], Fernandez-Barbero et al. [14]).

The fractal dimensions were calculated for the flocs in Fig. 7, by using a method (Vicsek [10]) designed to calculate the dimension of a single fractal: the number of particles $N(R)$ belonging to a fractal and lying within a circle of radius $R$ ($R$ less than the maximum dimension of the fractal) was evaluated and then $N(R)$ versus $R$ was plotted as a double logarithmic plot. From such an analysis it should be possible to deduce, for different conditions of particle and salt concentration, what regime of aggregation the system is in. The flocs that form are of course three dimensional, but the way the image is formed means that only the top quasi-two-dimensional plane is sampled. This means that the situation is more complicated than where the floc is constrained to lie at an interface and is therefore necessarily two-dimensional, as in many of the earlier works, Hurd and Schaefer [12], Stankiewicz et al. [13]. It is more akin to that of fat crystal networks recently analysed via optical microscopy (Narine and Marangoni [15]).
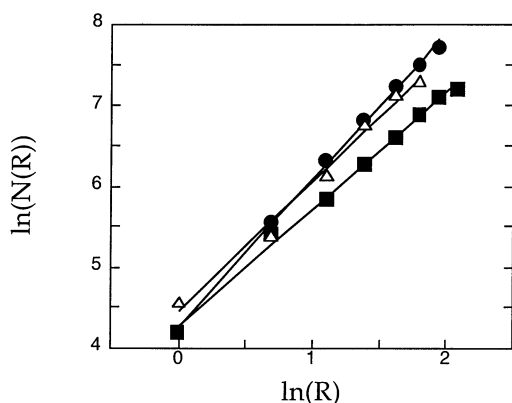
Fig. 8. Fractal dimensions calculated from the flocs shown in Figs. 7 and 9. The plot shows the number of particles contained within a radius $R$ as a function of $R$ for: ■ $= 0.078$ M $MgSO_4$; $\Delta = 0.25$ M $MgSO_4$ and ● = 'soft' particles shown in Fig. 9; all at a concentration of particles of $1 \times 10^{13}$ particles $cm^{-3}$.

Fig. 8 shows the results for this $N(R)$ versus $R$ analysis for the two flocs of Fig. 7. Although it is dangerous to draw too many conclusions from such a limited data set, it can be seen that the two slopes are somewhat different for the two different salt levels. The biggest aggregate in Fig. 7(a) has $\approx 1200$ particles in it, and the fractal dimension deduced from Fig. 8 is $1.45 \pm 0.05$. This can be compared with a value for $d$ of $1.6 \pm 0.05$ for the largest aggregate ($\sim 1700$ particles) in the higher salt case of Fig. 7(b). By watching how the aggregation occurs in the case of low salt, it is observed that the floc grows by individual particles sticking to the pre-existing cluster (although sometimes small clusters may also approach and stick). The salt concentration employed, 0.078 M, is close to the critical value at which aggregation first occurs and, as in the no-salt case, by no means every collision of a particle with a cluster leads to sticking. Thus the observations suggest that the mechanism operating is DLA, but not in the ideal sense of every encounter leading to sticking, but with a lower probability of aggregation than that. This may explain why the fractal dimension determined from Fig. 8 is lower than the theoretical predictions, although a much more substantial number of measurements would need to be carried out to confirm this suggestion.

When the salt concentration is raised to 0.25 M (Fig. 7(b)), a very different situation pertains. Because of the increased screening due to the salt, essentially every collision leads to sticking. Because of this a large number of small aggregates form. These clusters then move around and aggregate further, exactly the situation envisaged in the cluster-cluster aggregation model. The fractal dimensions ranged from 1.2 to 1.6 depending on the size of the aggregates. This is similar to the experimental results obtained by Stankiewicz et al., who showed that the fractal dimension increased as the size increased, also with a limiting value of 1.6 [13].

One possibility raised in the paper by Stankiewicz is the possibility that restructuring may occur after the floc first forms. The more open the structure which forms the more likely it is to occur for one arm to move and bump into another. If the sticking probability is high, then a new shape will form, whose fractal dimension no longer reflects the mechanism by which the original structure formed. In our work we saw evidence for this in the flocs formed from rather different 'soft' latex particles which lacked the outermost PMMA layer, but were also charge stabilised. Since the outer layer was rubber and hence soft, when contact between particles was made sticking always occurred (the $T_g$ of the rubber layer was $\sim -20°C$). Fig. 9 shows a typical floc for this system, grown at the same particle concentration as the earlier examples of $1 \times 10^{13}$ particles $cm^{-3}$, and with no added salt. It can be seen that the floc contains loops of particles, rather than dangling arms as in the earlier cases, giving an appearance overall of a network. This is consistent with collisions between the original arms having occurred, and the whole structure subsequently restructuring as the two arms stick together. Of course, it is additionally possible that the particles themselves are so soft that they deform individually; this will also have the effect of altering the fractal dimension determined, but it is hard to assess the impact of this as even this comparatively high resolution technique cannot follow the individual particles with this degree of detail.
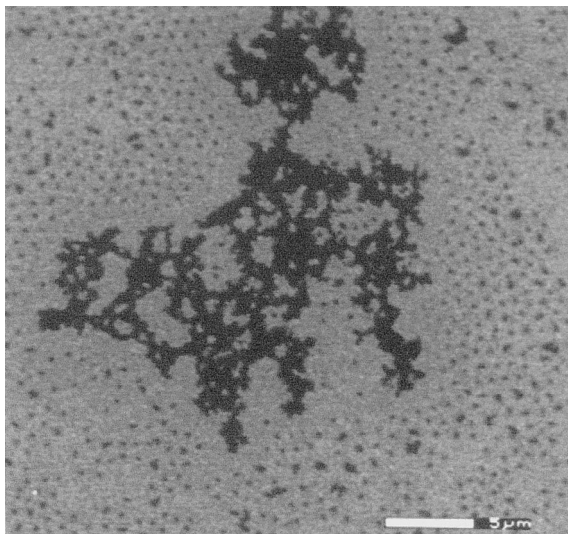
Fig. 9. Floc formed from 'soft' particles, i.e. those with a rubber outer layer.

The ESEM used in this way therefore opens up the possibility of a high resolution way of studying fractal structure evolution. Whereas the numbers obtained here should be regarded only as indicative of what can be done, several points can be noted. First, ESEM has the resolution, which light microscopy does not, to image individual latex particles. Thus the details of the encounters which occur —does a particle-particle collision lead to sticking or not? — can be directly obtained. Secondly, whereas previous work using electron microscopy to study fractal structures, Lin et al. [16], Brady and Ball [17] required dehydration prior to observation, and can only then observe what is likely to be a collapsed structure, ESEM permits the direct observation of the floc in its native state. What is observed is, however, clearly only the surface of a three-dimensional structure. Thus, unlike in many of the optical studies where a true 2 dimensional structure is formed by constraining the aggregation to occur at the air/water interface [12,13], there is no such constraint operational here although a three dimensional mass/number of particles cannot be obtained from the images. From this summary it can be seen how ESEM studies may contribute further to studies of the fractal nature of colloidal aggregation.

One caveat should be mentioned at this point. In the preceding paragraphs it has been implied that real time observations can be made as evaporation proceeds. This is of course true, but the observer must always be aware of the possibility of beam damage becoming a limiting factor. Beam damage is a ubiquitous problem for electron microscopists working on organic and many inorganic systems (but not in general metals). It transpires that in the ESEM the situation is in general worse than for conventional SEM. This is for two reasons. Firstly there is no conductive coating required for the surface of an insulator, as discussed in the introduction. This means that there is no protective layer to dissipate some of the incoming electrons' energy. Secondly, and probably more importantly, the various processes that occur when electrons interact with water molecules, leads to the formation of free radicals through the process known as radiolysis. These free radicals can be very deleterious for organic materials. If the exposure is continued for sufficiently long, the damage is easily visible.

As an example, away from the field of pure colloids, Fig. 10 shows a sequence of images during hydration of some substituted lyocell fibres. In the presence of water the fibres should swell, but this real effect may be obscured by beam-induced damage that can look broadly similar. In Fig. 10, by the end of 15 min exposure to beam plus water, there is substantial bubbling and swelling of most of the fibres (viewed end on). The effect is most severe at the left hand side of the figure where the way the electron beam dwells at the start of each line in the raster leads to a greater dose there than elsewhere. Consequently, right at the edge of the figure it seems as if all the originally distinct fibres have fused together. This effect appears to be general for cellulosic materials, and additional information can be found in refs [18–20].

The problem is that whereas the gross effects visible in Fig. 10 are readily detected, beam damage need not necessarily be so visible. FTIR spectroscopy has been used to quantify the extent of damage under different conditions, in this case for samples of polypropylene, [21]. This demonstrated that the presence of liquid water on the surface of
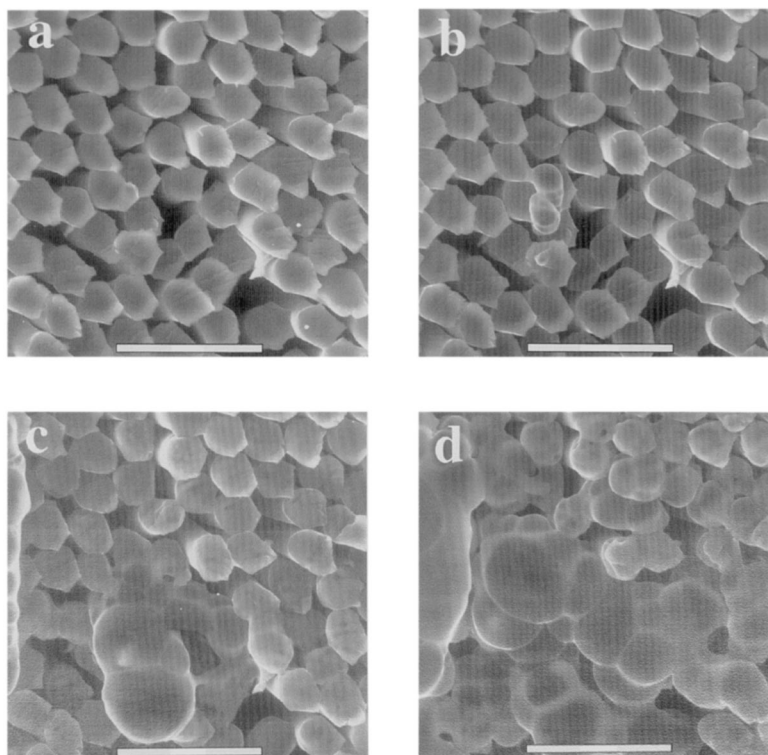
Fig. 10. Micrographs illustrating the visible changes to carboxymethyl-derivatised lyocell fibres in the ESEM under damaging conditions of the incident beam. The images show (a) undamaged fibres; (b) the start of bubbling; (c) continuing damage, with the effects of the beam raster pause evident down the left hand side of the image; and (d) the fibres obscured 15 min after the initiation of damage in (b). Scale bar represents 50 μm.

a sample renders the damage worse than if there is simply water vapour present in the chamber. This effect is presumed to be due to the ready mobility of radicals through the water layer, increasing the rate of polymer hydrolysis. This necessarily means that damage is likely to be an issue when imaging wet dispersions of PMMA latices, PMMA being notoriously susceptible to beam damage, and indeed used as an electron resist in e-beam lithography. Whereas this does not mean that any given image is necessarily artefactual, it does mean that caution must be exercised when sitting with the beam on any given area of a sample and watching how the structure evolves. Thus although one may have confidence that a conclusion such as that concerning the probability of sticking is valid, it does not mean that a video taken of a single floc is necessarily free of artefacts. It is for this reason that we have refrained from making

firm statements concerning rearrangements of one of the flocs comprising the soft particles; that is exactly the sort of situation where long term observations would need to be made. Nevertheless, as the work on damage to cellulose fibres has shown elsewhere, as long as one knows how long one can safely image a sample without significant beam damage occurring, then imaging over comparatively long periods can be made, [20,22].

## 3. Structure and aggregation of vinyl latices

### 3.1. Experimental

Both standard vinyl latices (supplied by ICI Paints) and those with starch incorporated were studied, to examine the effect of starch upon aggregation and coalescence. The starch was ei-

ther in the form of unmodified material, or derivatised potato starch. The effect of the addition of surfactant was also explored. The latices were imaged after spin coating onto glass stubs outside the ESEM, and carrying out a controlled pumpdown; images were also taken at increasing times thereafter up to 2 weeks, to follow the evolution of structure as the films dried. As in the above case, care has to be taken to avoid beam damage.

## 3.2. Results and discussion

Vinyl latices are very often used in paint formulations. As such it is desirable that the individual particles rapidly aggregate and coalesce followed

by interdiffusion across the initial particle boundaries occur to yield a film with good mechanical properties. The required stages in film formation are described in detail elsewhere, [23]. As formulation developments occur, it is crucial that alterations do not impede these various stages. Fig. 11 shows images taken during drying for a commercial vinyl latex to which 10% of native starch has been added during polymerisation. Fig. 11(b) shows two key features. First the individual particles have a very narrow size distribution compared with the standard commercial formulation (shown in Fig. 11(c and d)). However, although this might seem like an attractive advantage the particles show no tendency to coalesce even after 2 weeks of drying. This means
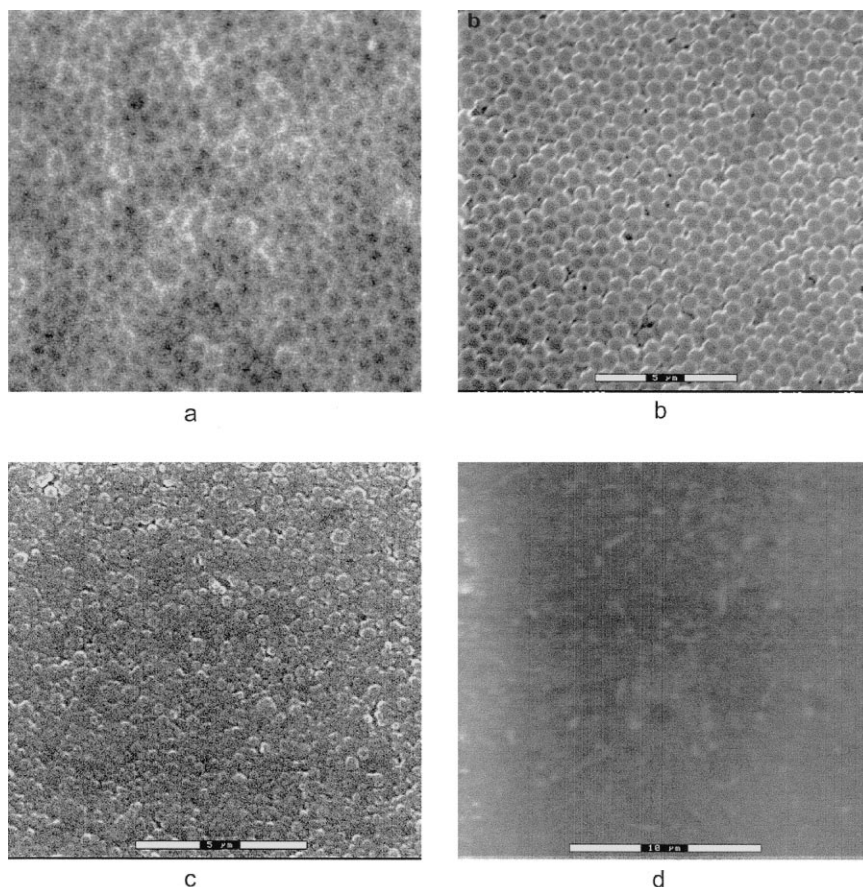


Fig. 11. ESEM images of vinyl latex with 10% native potato starch (a) 10 min and (b) 2 weeks after deposition; ESEM images of commercial vinyl (c) 10 min and (d) 2 weeks after deposition.
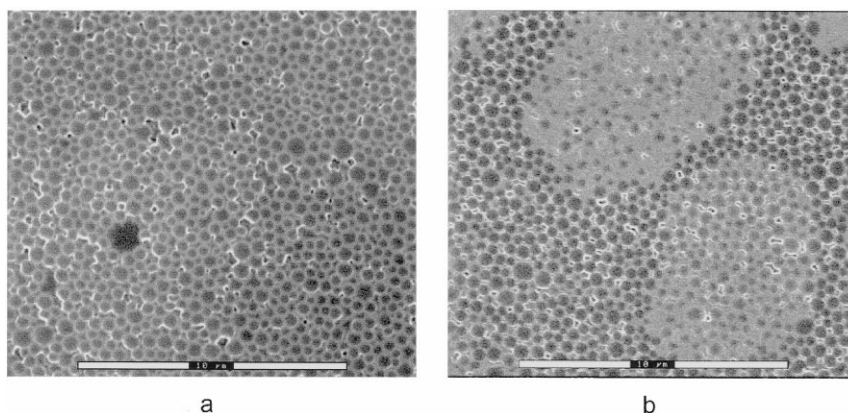
Fig. 12. ESEM images of vinyl latex with 10% modified potato starch (a) 10 min and (b) 3 weeks after deposition.

that the quality of the film is unacceptable. Exactly what role the native starch is playing cannot be assessed from this information alone, but it is clear that it is radically affecting the surfaces of the particles. This altered surface chemistry will then affect both the polydispersity and the interdiffusion.

If on the other hand the starch is chemically modified, so that the original granular structure is totally lost before addition, the response of the latex (the same base vinyl formulation) is rather different. Fig. 12 shows results for a latex formed with 10% of modified potato starch (it should be noted that the species from which the starch comes from also affects its behaviour). Although in this case both at early and late stages the films are fairly flat and particle deformation can be seen even at early times, after 3 weeks there are numerous imperfections still present in the film, although some particle coalescence has occurred. In the dry films there are therefore small cracks at some of the particle interfaces rendering the film of an unacceptable quality. The particle polydispersity is greater than in the case of the addition of unmodified starch.

As it is clearly some element of the surface chemistry that is being affected by the presence of the starch, the effect of the addition of a surfactant was also explored. Fig. 13 shows the results when surfactant is added to the sample containing the modified potato starch. The particle polydispersity is now even greater although the mean particle size is significantly smaller, but the main consequence is the apparently very rapid coalescence of the particles. After 1 h all particle boundaries have disappeared. However at much longer times a new effect is seen: regions of bright contrast slowly begin to appear on the surface. This effect is attributed to the slow exudation of excess surfactant to the surface to form pools upon it. This interpretation is confirmed by altering the level of surfactant addition, which reduces the amount of exudate which appears on the surface.

Although this is an incomplete story, it highlights the power of the ESEM for analysing the changing structure of latex films as water evaporation occurs. Because water loss does not occur due simply to the high vacuum conditions of observation, as in a conventional SEM, we can have confidence that the changes that are observed during drying are real and not artefactual. The high resolution images means both that information about particle polydispersity and the degree of particle coalescence can readily be obtained. In terms of identifying whether standard synthetic organic additives can be replaced by starch, it can be seen that good quality paint films can be obtained using such formulations. However, as one might expect, there is a complex interplay of many factors largely revolving around the alteration in surface chemistry: this affects both particle polydispersity during polymerisation, and ability to film form. Utilising the
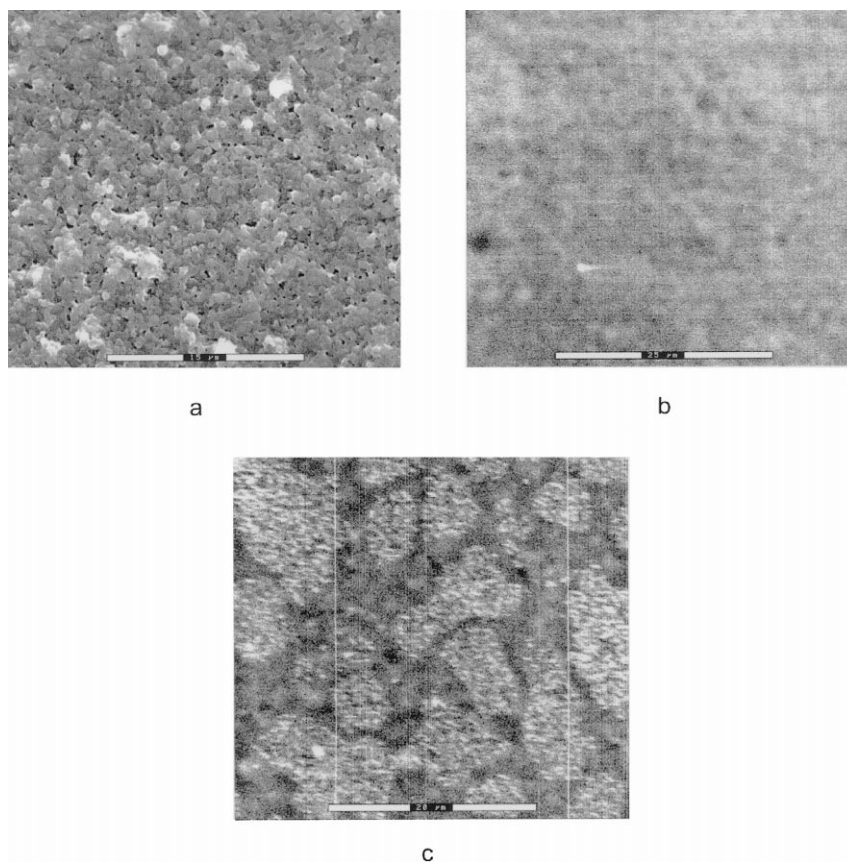
Fig. 13. ESEM images of vinyl latex with 10% modified potato starch plus 10% surfactant (a) 10 min and (b) 1 h and (c) 1 week after deposition.

ESEM means that these factors can be unambiguously determined, rather than simply relying on parameters such as film formation temperature or gloss as a quality determinant.

## 4. Film formation in the presence of hard inclusions

Finally, let us consider the situation when hard particles are also present. These might either be particles of a higher glass transition temperature than the remainder, and hence unable to participate in film formation, or an inorganic inclusion added for a variety of reasons. In an example of the former situation, in which ESEM was used in conjunction with ellipsometry [24], it was found that the presence of an increasing concentration of non-film forming particles led to an increase in the number of voids. This had the effect of increasing the total time taken for film formation. However the ability to image the particles directly in the ESEM enabled a distinction to be made between the situation where a void was associated with only one individual hard particle, from the situation in which a void is formed interstitially between several. In the latter case void closure was much harder. Consequently, when hard particles are present it is important to ensure a uniform distribution to minimise the risk of hard particle clusters.

In this section we will consider what happens when silica particles are added to an acrylic latex as a matting agent. The silica particles may them-
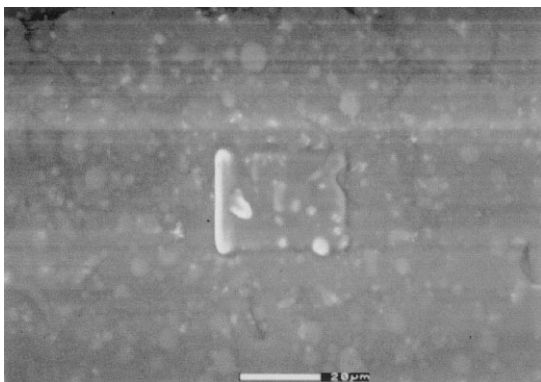
Fig. 14. Primary beam damage of a latex containing silica, imaged at 12 keV accelerating voltage. The sample was viewed at higher magnification and then the magnification reduced so that the fingerprint of the original raster can clearly be seen. Because the beam dwells slightly longer at the start of each line in the scan, the left-hand side of the raster is particularly badly damaged.

selves be agglomerates and porous and how effective they are as matting agents will obviously depend both on how they interact with the film-forming matrix and how they distribute themselves throughout the film.

### 4.1. Experimental

Two types of silica have been used. The first was a precipitated silica supplied by Crossfields and the second was a fumed silica obtained from Degussa. In the case of the former, the primary particles are typically $\sim 50$ nm in diameter. These aggregate to give a loose, porous structure with a broad distribution of particle sizes peaking at around 7 μm. The fumed silica has even smaller primary particles, $\sim 15$ nm in average diameter and again these aggregate via weak hydrogen bonds to give aggregates with a typical size of 10 μm.

These silica particles were dispersed in an aqueous acrylic latex of mean particle size $\sim 80$ nm; the disperson also contained a variety of additives to aid the film formation process. The concentration of silica particles was varied from 0.5–5% by weight. Experiments were carried out both during the drying process, and on the final dried films. Drying was carried out in situ follow-

ing an optimised pumpdown procedure, Cameron and Donald [5] to prevent premature dehydration. After the pumpdown, slow evaporation of the water was allowed to occur whilst imaging proceeded at a temperature typically of 8°C. Series of drying images were obtained by a gradual increase of the sample temperature. Once silica particles could be distinguished form the aqueous background, images were recorded every few minutes. A continuous transformation from a uniform-aqueous latex to a dried film in which the silica is clearly distinct was observed. This system proved quite susceptible to beam damage, as shown in Fig. 14. This figure shows a central rectangle which has been heavily irradiated at high magnification, and then the magnification reduced to expose the affected area. It can be seen (as in Fig. 10) that the damage is greatest at the left-hand side of the raster, where the dwell time of the beam at the start of each line in the raster is greatest. To reduce beam damage to an acceptable level, the accelerating voltage was reduced to 8 keV, and a short working distance used.

### 4.2. Results and discussion

Fig. 15 compares a drying sequence for matrices containing 2.5% fumed and precipitated silica. Firstly it is clear that the silica particles appear bright. This is not surprising since they are of higher atomic number than the matrix and, as in a conventional SEM, their backscattered emission is therefore higher. At the magnifications employed, the individual primary particles cannot be distinguished, although it is clear that the particles do have internal sub-structures present; this is particularly apparent in Fig. 15(c), where some large particles with internal structure are evident. The rather uniform size distribution of the fumed silica is readily seen, whereas the particles of the precipitated silica have irregular shapes and with some particles significantly larger than 10 μm present. The uniform structure of the fumed silica aggregates is thought to be due to the way they agglomerate through hydrogen bonding. In contrast, the precipitated silica remains as separate particles.
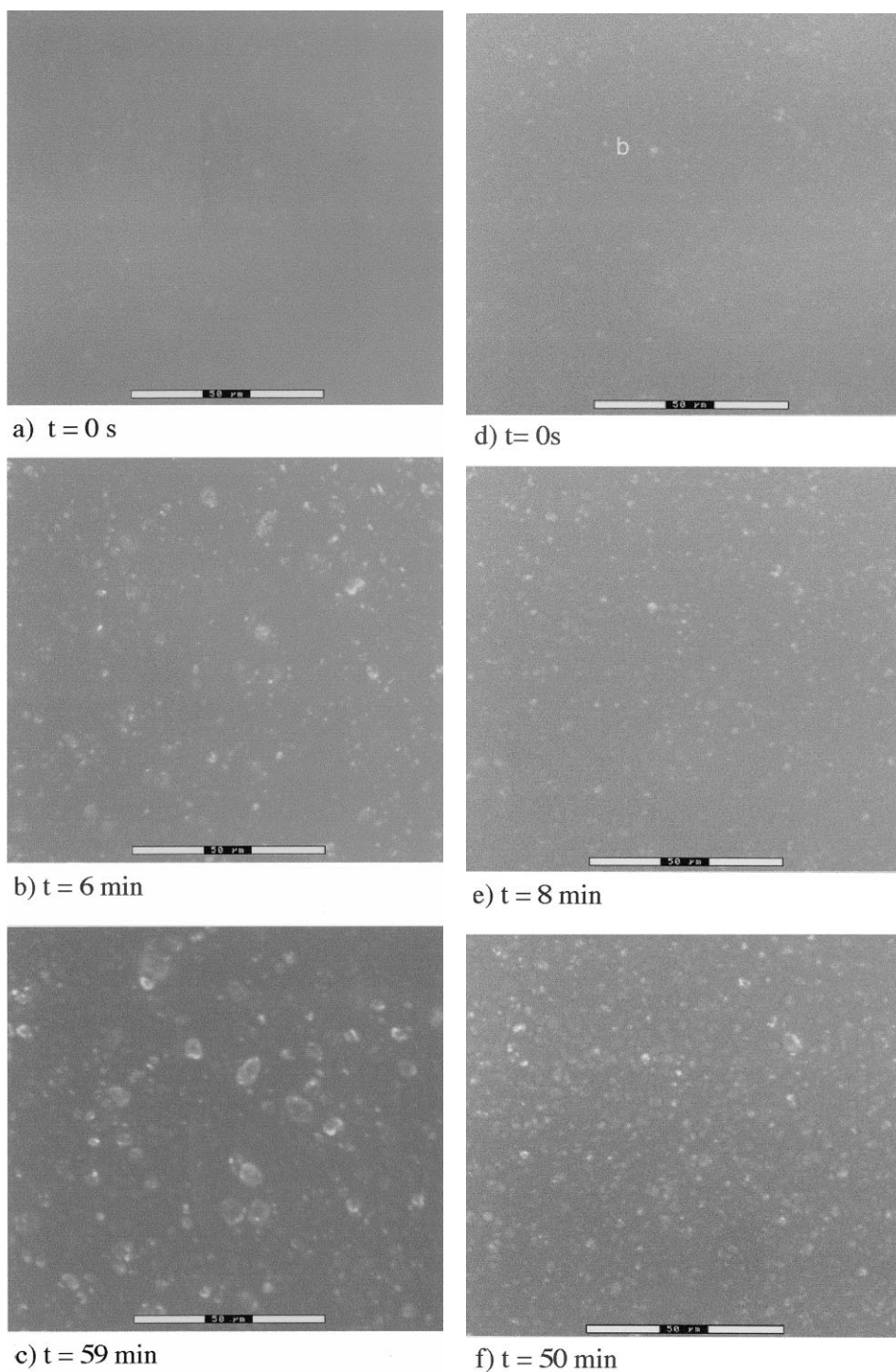
Fig. 15. Drying of films containing (a–c) precipitated and (d–f) fumed silica over 1 h: (a) $t = 0$ s; (b) $t = 6$ min; (c) $t = 59$ min; (d) $t = 0$ s; (e) $t = 8$ min and (f) $t = 50$ min.

Thus at a simple level, the contrast in the images of Fig. 15 can be understood. However, aside from the relative brightness of the silica particles there is a more subtle type of contrast visible in these images. As drying proceeds the background gets systematically darker. This is seen for both series of images in Fig. 15. In order to understand this we have to consider a little



a)



b)

Fig. 16. A comparison of the surface of dried films containing 1.25% (a) fumed and (b) precipitated silica.

more deeply the effect of water upon image formation. It was first noticed several years ago that a water layer surrounding a latex particle gave an anomalously high signal, which could not be explained by either of the standard SEM contrast mechanisms, namely topographic contrast (which arises primarily from the secondary electron signal) and atomic number contrast coming from the higher energy backscattered electrons [25]. Recent studies on contrast in oil/water emulsions has begun to cast light on this contrast [26]. Imaging of oil-in-water emulsions showed that the water phase looked bright, and this was maintained when the emulsion was inverted to form a water-in-oil emulsion, again demonstrating that the brightness was not a subtle topographic effect. Qualitatively the origin of the contrast can be attributed to the way in which the secondary electrons (which are by far the major constituent of the signal) lose energy as they travel through different materials.

Water can be considered as a wide band gap semiconductor, in the sense that there is a significant range of electron energies over which no inelastic collisions can occur to cause loss of energy to the secondary electrons as they travel through the material. Certainly by comparison with oils-which tend to have a degree of unsaturation which introduces the possibility of $\pi \rightarrow \pi^*$ transition energy levels occurring within the gap — there are fewer energy loss processes accessible to the secondaries. Hence a greater number of them will have sufficient energy to overcome the surface affinity and escape to be subsequently detected. It is for this reason that water looks bright compared with oils, or indeed a polymer matrix. For the images in Fig. 15, as the water content drops there will therefore be a systematic reduction in the electron signal escaping the surface and the sample will appear progressively darker during drying.

A second set of experiments was concerned with looking at the morphology of the dried films as a function of silica content. Fig. 16 compares samples with 1.25% of precipitated and fumed silica. It appears that there is more silica in the surface of the sample with the precipitated silica than that with fumed. This can be made more
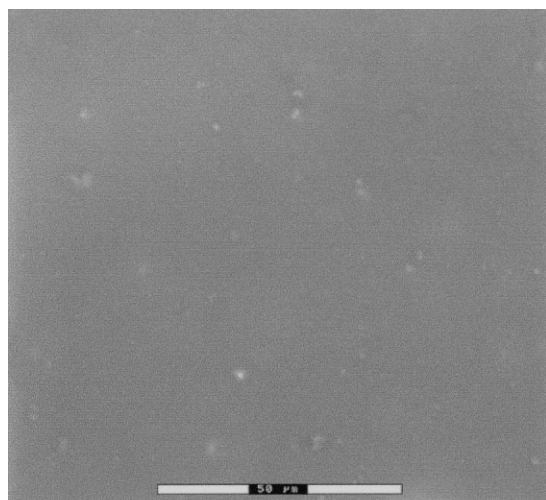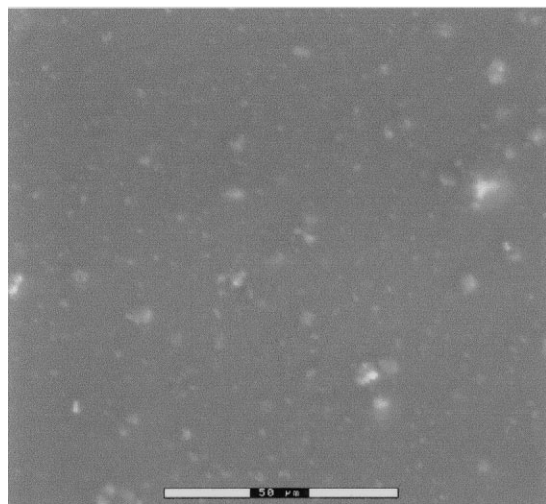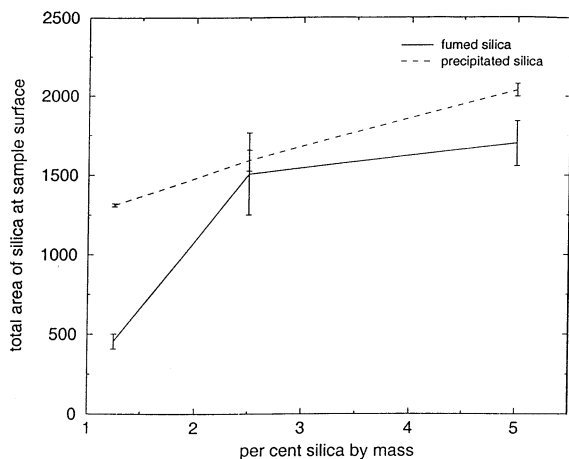
Fig. 17. Image analysis as a function of silica content comparing fumed and precipitated silica.

quantitative by carrying out image analysis on these and similar images as a function of overall silica content. The analysis was carried out by imposing a threshold grey level: pixels brighter than this threshold were presumed to be part of a silica particle, and all other pixels were treated as matrix. Because the particles contain internal morphology, this must be regarded as only a first approximation: for instance a convoluted shape may mean only some parts of the particle actually intersect the surface and are detected as 'silica'. The results of this analysis are shown in Fig. 17. It confirms that at low silica concentrations the surface occupancy of the samples with precipitated silica is higher than for the samples with fumed silica. However at higher concentrations, of $\sim 2\%$ silica and above, the fumed silica surface occupancy appears to reach a plateau value. Beyond this value for the bulk concentration it seems that the surface structure does not change any further.

Clearly this technique offers new possibilities of studying in detail the way the silica is distributed at the surface of a drying film. And since it is the nature of the surface which imparts the matting properties to the film, this may provide additional insight into how to optimise the silica type and properties. This brief example of the utilisation of image analysis also demonstrates how at least semi-quantitative information can be obtained from such images of the surface. Such a semi-quan-

titative approach permits a correlation between type of silica added (including its density) to the surface content. Further studies on surface roughness at the micron level can then rationalise the performance of different silicas.

However, it must be borne in mind that this technique can only reveal the top layer of a sample. Depth of field is good, as with conventional SEM, so that there is little difficulty associated with imaging a rough surface, but it is not possible to see through a significant layer of water, [27,28]. Thus, when wet colloidal dispersions are imaged there is a problem if none of the particles are sufficiently close to the surface for imaging. It also means that if the behaviour at the air/water interface is not typical of the bulk, this cannot be determined. For this reason it is highly desirable, whenever possible, to correlate information obtained from ESEM imaging with other techniques. In the case of the silica distribution discussed here, we are in the process of obtaining quantitative data on the distribution of the silica throughout the drying film via confocal microscopy, which permits optical sectioning through a thickness of up to $\sim 100$ μm. The confocal microscope has the opposite problem from the ESEM; it is difficult to obtain an absolute position for the surface of a rough film, through which silica particles may be protruding, but imaging below the surface is straightforward. The two techniques can therefore be seen to be highly complementary, and work is ongoing to correlate surface and sub-surface packing of the silicas.

## 5. Conclusions

This article has aimed to identify the many strengths of ESEM for the field of colloidal dispersions. Recognition of the fact that it is possible to image a wet sample in its natural state with resolution comparable to conventional (high vacuum) SEM, by dropping the temperature of the stage to slightly below ambient opens up a wide range of possibilities. Moreover, it is also possible to change the state of the sample, to move it between hydrating and dehydrating conditions, by modest changes in temperature or, less conve-

niently, chamber pressure. Thus dynamic experiments can readily be carried out. As long as beam damage is not an issue, it then becomes possible to follow dynamic changes in the state of a sample, illustrated here by following aggregation of latex particles. In other examples, outside the scope of this article, it is possible even to follow chemical reactions induced by the presence of water, as in the hydration of cement and its components, [29–33], as well as physical changes as can occur during the swelling of cellulose fibres, [20,22].

The utilisation of ESEM in this field is still in its infancy. It is clear that this in part has been because of a lack of availability of this new generation of instruments, but it is also due to a failure by some to recognise the need to maintain careful control over the state of hydration at all times via appropriate combinations of pressure and sample temperature. It is to be hoped that now so many of these fundamental issues have been clarified, we will see an explosion of activity in the field of colloids as the instrument's potential is more widely appreciated. It can be anticipated that new novel applications will be developed as the community grows.

## Acknowledgements

## References

[1] A.M. Donald, Curr Opin. Colloid Interface Sci. 3 (1998) 143–147.

[2] G.D. Danilatos, Adv. Electron. Electron Phys. 71 (1988) 109–250.

[3] A.L. Fletcher, B.L. Thiel, A.M. Donald, J. Phys. D 30 (1997) 2249–2257.

[4] B. Thiel, I.C. Bache, A.L. Fletcher, P. Meredith, A.M. Donald, J. Microsc. 187 (1997) 143–157.

[5] R.E. Cameron, A.M. Donald, J. Microsc. 173 (1994) 227–237.

[6] C. He, A.M. Donald, Langmuir 12 (1996) 6250–6256.

[7] G.C. Jeffrey, R.H. Ottewill, Colloid Polym. Sci. 266 (1988) 173.

[8] D.A. Weitz, Phys. Rev. Lett. 54 (1985) 1416.

[9] T.A. Witten, L.M. Sander, Phys. Rev. B 28 (1986) 5686.

[10] T. Vicsek, Fractal Growth Phenomena, World Scientific Publishing, Singapore, 1989.

[11] P. Richetti, J. Prost, P. Burois, J. Phys. Lett. 45 (1984) 1137.

[12] A.J. Hurd, D.W. Schaefer, Phys. Rev. Lett. 54 (1985) 1043–1046.

[13] J. Stankiewicz, M.A.C. Vilchez, R.H. Alvarez, Phys. Rev. E 47 (1993) 2663–2668.

[14] A. Fernandez-Barbero, M. Caberizo-Vilchez, R. Martinez-Garcia, R. Hidalgo-Alvarez, Phys. Rev. E 53 (1996) 4981–4989.

[15] S.S. Narine, A.G. Marangoni, Phys. Rev. E 59 (1999) 1908–1920.

[16] M.Y. Lin, H.M. Lindsay, D.A. Weitz, R.C. Ball, R. Klein, P. Meakin, Nature 339 (1989) 360–362.

[17] R.M. Brady, R.C. Ball, Nature 309 (1984) 225–229.

[18] J.G. Sheehan, L.E. Scriven, in: TAPPI/Coating Conference, 1991; pp. 337–383.

[19] P. Forsberg, P. Lepoutre, Scanning Microsc. 8 (1994) 31–34.

[20] L. Jenkins, A.M. Donald, Scanning 19 (1997) 92–97.

[21] S. Kitching, A.M. Donald, J. Microsc. 190 (1998) 357–365.

[22] L.M. Jenkins, A.M. Donald, Text Res. J., in press (1999).

[23] J.L. Keddie, Mater. Sci. Eng. R21 (1997) 101–170.

[24] J. Keddie, P. Meredith, R. Jones, A. Donald, Langmuir 12 (1996) 3793–3801.

[25] P. Meredith, A.M. Donald, J. Microsc. 181 (1996) 23–35.

[26] D.J. Stokes, B.L. Thiel, A.M. Donald, Langmuir 14 (1998) 4402–4408.

[27] J. Shah, R. Durkin, in: Inst. Phys. Conf. Ser., EMAG 91 Bristol, 1991, pp. 161–164.

[28] I.C. Bache, PhD Thesis, University of Cambridge, 1999.

[29] K.O. Kjellsen, H.M. Jennings, Adv. Cem. Bas. Mat. 3 (1996) 14–19.

[30] K. Sujata, H.M. Jennings, J. Am. Ceram. Soc. 75 (1992) 1669–1673.

[31] D.A. Lange, K. Sujata, H.M. Jennings, Ultramicroscopy 37 (1991) 234–238.

[32] P. Meredith, A.M. Donald, K. Luke, J. Mater. Sci. 39 (1995) 1921–1930.

[33] C. Hall, W.D. Hoff, S.C. Taylor, M.A. Wilson, B.-G. Yoon, H.W.-K. Reinhardt, M. Sororo, P. Meredith, A.M. Donald, J. Mater. Sci. Lett. 14 (1995) 1178–1181.